Bremsstrahlung, transition, and Cherenkov radiation by laser filaments

A. M. Zheltikov
Department of Physics and Astronomy, Texas A&M University, College Station, Texas 77843, USA;
Physics Department, M.V. Lomonosov Moscow State University, Moscow 119992, Russia;
and Russian Quantum Center, Skolkovo, Moscow Region 143025, Russia

(Received 12 April 2021; revised 4 July 2021; accepted 16 July 2021; published 12 October 2021)

Cherenkov radiation is one of the central effects in relativistic electrodynamics, which lends its name to a vast class of optical phenomena in which a moving source emits off-axis radiation, giving rise to a signature Cherenkov emission cone. When a radiation source is confined to a finite path, however, translational symmetry of its motion is removed, giving rise to edge effects that modify the canonical picture of conical emission. Here, we focus on one class of such edge effects as the key to understanding the properties of secondary radiation by laser-induced filaments. Charge-current transients near the edges of laser filaments are shown to couple Cherenkov emission to bremsstrahlung and transition radiation, giving rise to filament-length-sensitive features in the radiation field structure. We present a unified description of this class of radiation phenomena with a continuous analytical crossover from the subluminal to the superluminal setting of radiating currents and with the low-frequency cutoff in the radiation spectrum defined by the filament length.

DOI: 10.1103/PhysRevA.104.043509

I. INTRODUCTION

Laser-induced filamentation (LF) is one of the most remarkable effects in ultrafast optics [1,2] that reveals unique scenarios of nonlinear space-time wave dynamics [3–5], provides a source of bright multiband supercontinua [6–9], and enables a high-throughput compression of high-peak-power laser pulses to few-cycle field wave forms [10,11]. Lying at the interface between nonlinear optical science and ultrafast laser-plasma (LP) physics, research into laser filamentation reveals new aspects of laser–plasma interactions [12–16] and offers means to probe and eventually resolve laser-plasma nonlinearities related to bound-state electrons, ultrafast laser-induced ionization, and laser-plasma charge-carrier dynamics.

Ultrafast nonlinearities of ponderomotively and ionization-driven plasma currents have been shown to be central for understanding low-frequency, THz-to-microwave radiation by laser filaments [12,17]—an effect that brings the promise of bright THz-to-microwave sources for a vast range of applications [18], including medical imaging, safety screening, remote sensing communication technologies, material characterization, high-speed solid-state optoelectronics [19–21], laser-plasma particle acceleration [22], optical spintronics [23], and laser valleytronics [24,25]. Comprehensive models of laser-driven plasma currents have proven their high explanatory power [1,2,12–17], providing useful insights into many of the key properties of THz generation in LF or LP experiments. As a powerful insight, ponderomotively driven longitudinal plasma currents have been shown [12,13,17] to provide a source of bright transition–Cherenkov-type emission of THz radiation by laser filaments, offering an elegant explanation for many of the properties of THz radiation observed in LF experiments.

The question as to whether the same physical mechanisms can give rise to radiation at even lower, microwave frequencies, as detected in recent LP and LF studies [26–31], is far from trivial. Indeed, the spectrum of the low-frequency LP or LF output in some of the recent studies extends well beyond the plasma frequency cutoff, bringing up questions regarding the overall setting whereby superluminal [12] or subluminal [17,32] plasma currents can emit radiation at wavelengths much longer than the transverse size of the LP source.

Here, we seek to address these questions by examining representative generic models of electric-current wave forms in LFs and LPs, providing sources of low-frequency, THz-to-microwave secondary radiation. An analysis presented below in this paper shows that the edge effects inherent in the LF setting tend to couple Cherenkov radiation emitted by such currents to bremsstrahlung and transition radiation, often making these three types of radiation physically indistinguishable. Resorting to an evanescent-field extension of the Cherenkov effect to subluminal electric currents, we provide a unified description of low-frequency radiation by sub- and superluminal plasma currents with a continuous analytical crossover from the superluminal to the subluminal picture of bremsstrahlung-transition-Cherenkov radiation. In this laser-plasma interaction scenario, long-wavelength radiation builds up outside the laser plasma, unfolding at spatial scales much larger than the transverse size of the LP source. Central to this physical setting is an interference of electromagnetic traveling waves emitted by impulsively driven transient currents near the LP or LF edges, which combine into a far-field radiation pattern whose low-frequency cutoff is defined by the LP or LF length and whose spectral and spatial properties are in agreement with experimental studies.

II. CHERENKOV RADIATION: FRANK-TAMM TREATMENT

We start with a generic model of an electric current $\mathbf{j}$ induced by an electric charge e moving along an infinite straight line with a constant speed $\mathbf{v}$:

$$\mathbf{j} = e\mathbf{v}\delta(\mathbf{r} - \mathbf{v}t), \tag{1}$$

where $\mathbf{r}$ is the radius vector and t is time.

With the z axis chosen along $\mathbf{v}$, the Cartesian components of $\mathbf{j}$ are

$$j_x = j_y = 0,\ j_z = ev\delta(z - vt). \tag{2}$$

We search for the radiation field of such a current by following the Frank-Tamm treatment [33,34] in solving the set of equations for the Fourier transforms of the fields and potentials:

$$\nabla^2\mathbf{A}_\omega + k_0^2 n^2 \mathbf{A}_\omega = -\frac{4\pi}{c}\mathbf{j}_\omega, \tag{3}$$

$$\nabla^2\phi_\omega + k_0^2\phi_\omega = -\frac{4\pi}{n^2}\rho_\omega, \tag{4}$$

$$\mathbf{H}_\omega = \nabla \times \mathbf{A}_\omega, \tag{5}$$

$$\mathbf{E}_\omega = -\nabla\phi_\omega - \frac{i\omega}{c}\mathbf{A}_\omega, \tag{6}$$

Here, $\mathbf{E}_\omega$ and $\mathbf{H}_\omega$ are the Fourier transforms of the electric and magnetic fields, ϕ_ω and $\mathbf{A}_\omega$ are the Fourier transforms of the scalar and vector potentials, ρ_ω and $\mathbf{j}_\omega$ are the Fourier transforms of the charge density and the electric current, $k_0 = \omega/c$, c is the speed of light in vacuum, and $n = n(\omega)$ is the refractive index.

The Fourier transform of the current j_z as defined by Eq. (2) is

$$j_z(\omega) = e/(2\pi)\exp(-i\omega z/v)\delta(x)\delta(y), \tag{7}$$

or, in cylindrical coordinates ρ, ϕ, z,

$$j_z(\omega) = e/(2\pi^2\rho)\exp(-i\omega z/v)\delta(\rho). \tag{8}$$

We search for the solutions as suggested by the cylindrical symmetry and the z-dependent phase of the current (8):

$$A_\rho = A_\phi = 0, \tag{9}$$

$$A_z(\omega) = e/(2c)a(\rho,\omega)\exp(-i\omega z/v). \tag{10}$$

Plugging Eqs. (9) and (10) into Eq. (3) yields [33,34]

$$\frac{\partial^2 a}{\partial\rho^2} + \frac{1}{\rho}\frac{\partial a}{\partial\rho} + s^2 a = -\frac{4}{\pi\rho}\delta(\rho) \tag{11}$$

with

$$s^2 = \frac{\omega^2}{v^2}(\beta^2 n^2 - 1)$$

and $\beta = v/c$.

The general solution for $u(\rho,\omega)$ that satisfies Eq. (11) everywhere except for the pole at $\rho = 0$ is [35]

$$\begin{aligned} a(\rho,\omega) &= c_1 H_0^{(1)}(s\rho) + c_2 H_0^{(2)}(s\rho) \\ &= c_1 H_0^{(1)}(i\sigma\rho) + c_2 H_0^{(2)}(i\sigma\rho), \end{aligned} \tag{12}$$

where $H_0^{(1)}(\xi)$ and $H_0^{(2)}(\xi)$ are the Hankel functions of the first and second kind, c_1 and c_2 are constants, and $\sigma^2 = -s^2$.

For low v, such that $\beta n < 1$ and $s^2 < 0$, σ is real, allowing the solution for a to be written as

$$a = iH_0^{(1)}(i\sigma\rho). \tag{13}$$

In the limit of $\sigma\rho \gg 1$, the radiation field decays exponentially with ρ,

$$a \approx \left(\frac{2}{\pi c\rho}\right)^{1/2}\exp(-\sigma\rho). \tag{14}$$

In this regime, the fields induced by the current (2) are purely evanescent, giving rise to no radiation in the far field.

For high v, on the other hand, such that $\beta n > 1$ and s is real, Eq. (12) yields an outgoing cylindrical wave with

$$a = -iH_0^{(2)}(s\rho) \quad \text{for} \quad \omega > 0 \tag{15}$$

and

$$a = iH_0^{(1)}(s\rho) \quad \text{for} \quad \omega < 0. \tag{16}$$

In the limit of $s\rho \gg 1$, the only nonzero component of the vector potential is

$$A_z(\omega) \approx \frac{-ie}{c(2\pi s\rho)^{1/2}}\exp\left(-i\omega\frac{z}{v} - is\rho + i\frac{\pi}{4}\right). \tag{17}$$

Introducing the Cherenkov angle, $\cos\theta_0 = 1/(\beta n)$, it is convenient to rewrite Eq. (17), correcting a series of typos existing in the literature, as

$$A_z(\omega) \approx \frac{-ie}{c(2\pi s\rho)^{1/2}}\exp\left[-i\frac{\omega}{c}n(z\cos\theta_0 + \rho\sin\theta_0) + i\frac{\pi}{4}\right]. \tag{18}$$

Equation (18) defines radiation field whose wave front propagates at an angle ϑ_0 relative to the z axis [Fig. 1(a)], thus reproducing the celebrated result for the Cherenkov emission cone [33–37].

The nonvanishing components of the radiation field as defined by Eqs. (3)–(6) are

$$E_\rho = -\frac{e}{2\beta c}\int_{-\infty}^{\infty}\frac{1}{n^2}\frac{\partial a(\rho,\omega)}{\partial\rho}\exp\left[i\omega\left(t - \frac{z}{v}\right)\right]d\omega, \tag{19}$$

$$E_z = \frac{ie}{2c^2}\int_{-\infty}^{\infty}\left(\frac{1}{\beta^2 n^2} - 1\right)a(\rho,\omega)\omega\exp\left[i\omega\left(t - \frac{z}{v}\right)\right]d\omega, \tag{20}$$

$$H_\phi = -\frac{e}{2c}\int_{-\infty}^{\infty}\frac{\partial a(\rho,\omega)}{\partial\rho}\exp\left[i\omega\left(t - \frac{z}{v}\right)\right]d\omega. \tag{21}$$

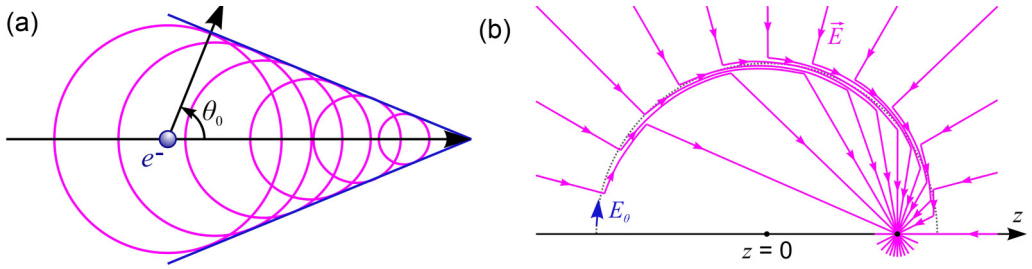

FIG. 1. (a) Cherenkov radiation of a relativistic charge moving with a speed v in a medium with a refractive index n as a result of interference of spherical waves (pink circles) emitted at each point along the path of the particle. (b) Purcell's solution [52] for the field of a charge that instantaneously starts moving at $z = 0$. The radiation field with the only electric-field component E_θ is shown against the electrostatic field induced by the charge. A segment of a circle centered at $z = 0$ with a radius of ct/n is shown with the dotted line.

III. CHERENKOV RADIATION IN RELATIVISTIC PHYSICS AND NONLINEAR OPTICS

In its original, relativistic-physics version [34–36], Cherenkov radiation refers to a radiation of a relativistic charge [Figs. 1(a) and 2(a)] that moves in a medium with a speed, v_c, higher than the phase velocity of radiation it emits, $v_c > u = c/n(\omega)$. Originally meant to refer to radiation by relativistic charged particles, in the laser era, the term "Cherenkov radiation" has absorbed a much broader sense, lending its name to a vast class of radiation phenomena in which a source of radiation, moving with a speed above c/n, emits an off-axis radiation, giving rise to a signature Cherenkov emission cone.

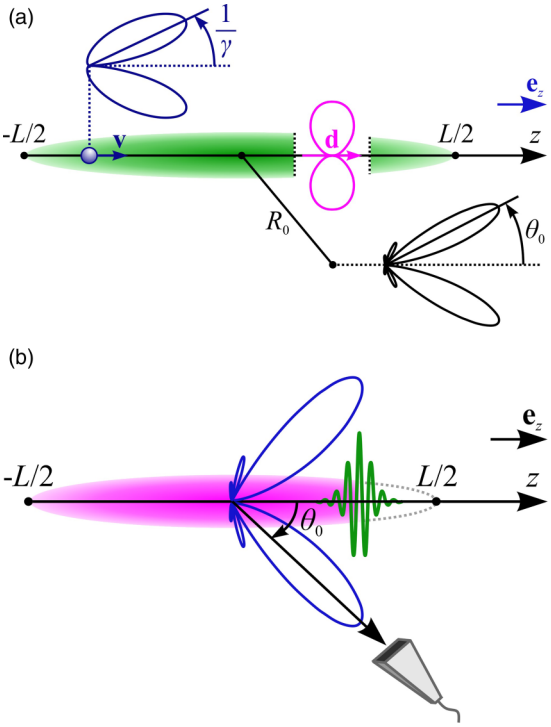

FIG. 2. (a) An electric charge moving with a speed $\mathbf{v}$ along a laser filament of length L. Also shown are the radiation patterns of bremsstrahlung emitted by this charge as it instantaneously starts moving at $z = -L/2$ (blue line), an electric dipole $\mathbf{d} = eL\mathbf{e}_z$ (pink line), and the entire finite-length filament (black line), with $\mathbf{e}_z$ being the unit vector along the z axis and R_0 being the distance between the filament and a far-field observation point. (b) Bremsstrahlung-transition Cherenkov radiation by a laser filament. An ultrashort laser pulse (green line) induces an ultrafast ionization of an initially neutral gas (pink shading), giving rise to a steep ionization front (the boundary between the pink shading and the unshaded area), which propagates through the gas in the wake of the laser driver. Shown with a blue line is the radiation pattern of secondary radiation emitted by a laser filament extending from $z = -L/2$ to $z = L/2$.

Nonlinear optics is particularly rich with radiation phenomena in which a source—a driver pulse or laser-induced nonlinear polarization—rides through a medium faster than $c/n(\omega_s)$, but allows phase matching with an off-axially radiated optical field at frequency ω_s. Examples include, but are in no way limited to, the Cherenkov harmonic generation in waveguides and photonic crystals [38–42], Cherenkov emission of THz radiation in electro-optical materials [43,44], Cherenkov radiation by optical solitons [45–48], and, more recently, Cherenkov radiation of THz field wave forms by laser filaments [12,17,32].

Specifically, in a laser filament, an ultrashort laser driver [green line in Fig. 2(b)] induces an ultrafast ionization of an initially neutral gas [pink shading in Fig. 2(b)], giving rise to a steep ionization front [the boundary between the pink shading and the unshaded area in Fig. 2(b)], which propagates through the gas in the wake of the laser driver. Transient plasma currents induced via such laser-driven ultrafast ionization provide a source of low-frequency secondary radiation, giving rise to THz and sub-THz radiation [12,17,32]. The electrons that constitute such currents move at speeds well below the speed of light. The laser-induced ionization front that drives these currents, however, propagates through the gas along with the laser pulse [Fig. 2(b)]. The speed of this ionization front can be close to or even higher than the phase velocity of THz/microwave radiation, giving rise to THz or microwave radiation patterns in the form of a celebrated Cherenkov emission cone [Fig. 2(b)], offering a consistent explanation to the conical emission of THz radiation observed in many experiments on laser-induced filamentation [13,28,29,31,32].

IV. RADIATION BY A FINITE FILAMENT OF CURRENT

With this picture of secondary radiation by plasma currents in mind, we consider an electric current $\mathbf{j}$ induced by an

electric charge q moving with a constant speed $\mathbf{v}$ along a straight line of finite length L [Fig. 2(a)]. With the z axis chosen along $\mathbf{v}$, as before, the Cartesian components of $\mathbf{j}$ are

$$j_x = j_y = 0,\ j_z = ev\delta(x)\delta(y)\delta(z - vt) \tag{22}$$

for $-L/2 \leqslant z \leqslant L/2$ and $j_z = 0$ otherwise.

The Fourier transform of j_z as defined by Eq. (22) is

$$j_z(\omega) = [e/(2\pi)]\delta(x)\delta(y)\exp(-i\omega z/v), \tag{23}$$

for $-L/2 \leqslant z \leqslant L/2$ and $j_z(\omega) = 0$ otherwise.

The solution for the vector potential can then be written as

$$A_\omega(\rho, z) = \frac{e}{2\pi c}\int_{-L/2}^{L/2}\frac{1}{R}\exp\left[-i\frac{\omega}{v}(\zeta + \beta nR)\right]d\zeta, \tag{24}$$

where $R^2 = \rho^2 + (z-\zeta)^2$.

In the far field, $R \gg L$, $R = R_0 - \zeta\cos\theta$, where $R_0^2 = \rho^2 + z^2$ and $\cos\vartheta = z/R_0$ [Fig. 2(a)], Eq. (24) yields

$$A_\omega = \frac{e}{2\pi cR_0}\exp\left(-\frac{i\omega n}{c}R_0\right)\int_{-L/2}^{L/2} \times \exp\left[-\frac{i\omega}{v}(1 - \beta n\cos\theta)\xi\right]d\xi = e\beta a_\omega Q(\omega, \theta, L), \tag{25}$$

$$a_\omega = \frac{1}{\pi R_0\omega}\exp\left(-\frac{i\omega n}{c}R_0\right), \tag{26}$$

$$Q(\omega, \theta, L) = \frac{\sin\left[\frac{\omega L}{2v}(1 - \beta n\cos\theta)\right]}{1 - \beta n\cos\theta}. \tag{27}$$

This solution for $\mathbf{A}_\omega$, as well as the pertinent solutions for the $\mathbf{E}$ and $\mathbf{H}$ fields, can be recovered [49] by integrating Eqs. (18)–(21) in z with the angular spectrum of the radiating current, $j(\omega, k)$ as dictated by Eq. (22) instead of $j(\omega, k) = ev\delta(k–k_c)$, with $k_c = k_0 n\cos\theta_0 = \omega/v$, as would be the case for an infinite-length radiating current as described by Eqs. (1) and (2).

When applying Eqs. (22)–(27) to the analysis of secondary radiation by laser filaments, the picture that we have in mind is that of an ultrashort laser driver with a central frequency ω_0 [green line in Fig. 2(b)], inducing an ultrafast ionization of an initially neutral gas or a solid [pink shading in Fig. 2(b)], giving rise to a steep ionization front [the boundary between the pink shading and the unshaded area in Fig. 2(b)], which propagates through the gas in the wake of the laser driver. Transient plasma currents induced via such laser-driven ultrafast ionization provide a source of low-frequency secondary radiation [12,17], leading to THz and sub-THz generation [Figs. 2(a) and 2(b)]. Although the laser pulse leaves plasmas in its wake along its trajectory, the plasma cutoff at $\omega = \omega_p$, ω_p, being the plasma frequency, is not a concern, because the driver pulse propagates in an initially neutral medium, with the ionization front riding on its back, while secondary radiation that this ionization front emits propagates outside the laser-induced plasma that the driver pulse leaves behind [Figs. 2(a) and 2(b)]. Because the speed of the radiation source in such a setting, $v = c/n_g(\omega_0)$, is determined by the group index of a spatially uniform neutral medium at frequency ω_0, while the phase velocity of the radiated wave, $u = c/n(\omega)$, is controlled by the refractive index of a spatially uniform neutral medium at frequency ω, both v and u can be treated as spatially uniform, z-independent parameters.

As perhaps the most striking result, radiation emitted by the current (22) is no longer a prerogative of superluminal, $v > c/n$ charges, but can also be emitted by subluminal currents, i.e., currents with $v < c/n$. Mathematically, radiation by such subluminal currents becomes possible due to the loss of the translational symmetry of the radiating source [cf. Eqs. (2) and (22)] and can be viewed as an evanescent-wave extension of Eqs. (18) of the Frank-Tamm theory, with the transverse field profile as described by Eqs. (13) and (14). With such an extension, the crossover from the superluminal to the subluminal regime of charge-current radiation is continuous and analytical. As an interesting insight, solutions for the radiation emitted by a subluminal finite-L current (22) can be recovered from the Frank-Tamm solutions (18)–(21) by extending the definition of $\sin\vartheta_0$ to $\beta n < 1$ via $\sin\vartheta_0 = i[1/(\beta n)^2–1]^{1/2}$ [49].

To gain insight into these results, we recast integration in Eq. (25) to represent A_ω as a sum

$$A_\omega = \Phi(\beta, \theta, z = L/2) - \Phi(\beta, \theta, z = -L/2), \tag{28}$$

$$\Phi(\beta, \theta, z) = -ia_\omega\exp[i\varphi(z)]b(\beta, \theta), \tag{29}$$

$$b(\beta, \theta) = \frac{e\beta}{1 - \beta n\cos\theta}, \tag{30}$$

$$\varphi(z) = \frac{\omega z}{v}(1 - \beta n\cos\theta). \tag{31}$$

The spectral intensity of this radiation field is

$$S(\omega, \theta, L) \propto \frac{e^2\beta^2}{4\pi^2 cR_0^2}[Q(\omega, \theta, L)]^2\sin^2\theta, \tag{32}$$

leading to

$$S(\omega, \theta, L) \propto \frac{1}{4\pi^2 cR_0^2}[b(\beta, \theta)]^2\sin^2\left[\varphi\left(\frac{L}{2}\right)\right]\sin^2\theta, \tag{33}$$

or

$$S(\omega, \theta, L) \propto \frac{1}{R_0^2}J_B(\theta)\sin^2\left[\varphi\left(\frac{L}{2}\right)\right], \tag{34}$$

where

$$J_B(\theta) = \frac{e^2\beta^2}{4\pi^2 c}\frac{\sin^2\theta}{(1 - \beta n\cos\theta)^2} \tag{35}$$

is readily recognizable as the spectral intensity of bremsstrahlung per unit solid angle [37,50]. For $n \simeq 1$ and $\gamma = 1/(1–\beta^2)^{1/2} \gg 1$, $J_B(\vartheta) \simeq [(e\beta)^2/(4\pi^2 c)]\gamma^2\vartheta^2/(1 + \gamma^2\vartheta^2)^2$ reaches its maximum at $\vartheta \simeq 1/\gamma$, leading to a radiation pattern as sketched by the blue line in Fig. 2(a).

V. CHERENKOV EMISSION CONE AND PHASE MATCHING

Setting $\beta = 1$ and $n = 1$, reduces Eqs. (28)–(35) to

$$S(\omega, \theta, L) \propto \frac{\sin^2\theta}{(1-\cos\theta)^2}\sin^2\left[\frac{\omega L}{2c}(1-\cos\theta)\right]. \quad (36)$$

Equation (36) thus not only assumes that the radiation source moves at the speed of light in vacuum, $v = c$, but also entirely neglects, via $n(\omega) = 1$, the refraction of the medium (the difference of the phase velocity of electromagnetic radiation in a medium from c) and its dispersion (the frequency dependence of the refractive index). However unphysical they might seem, these simplifications prove adequate to certain regimes of THz generation by laser filaments. In laser filamentation, an ultrashort laser pulse propagating through a transparent medium induces an ultrafast ionization of this medium, giving rise to a steep front of photoionization, which rides on the back of the pulse, providing a source of THz radiation [Fig. 2(b)]. Because the photoionization front is coupled to a laser pulse, its speed v is close to the group velocity of the laser pulse, whose leading edge sees a neutral medium before ionization. In the case of laser filamentation in a gas medium, v is very close to c. The phase velocity of Cherenkov radiation in this setting is $u = c/n(\omega)$. Within a limited bandwidth, refraction of the medium and its dispersion can be neglected, in a rough approximation, $n(\omega) \approx 1$ and $u \approx c$, leading to Eq. (36). This approximation has proven useful, providing an adequate fit for the angular profiles of THz radiation in laser-filamentation experiments [13,31,32,51].

Within a broader bandwidth, however, a consistent, causal treatment of secondary radiation by laser filaments needs to adequately account for the subluminality of the radiation source, $v < c$, as well as the refraction of the medium and its dispersion, leading to $u = u(\omega) = c/n(\omega)$ and bringing causality into a picture. Equations (28)–(35) provide an adequate framework for such a treatment. The denominator $1-\beta n(\omega)\cos\theta$ in Eqs. (30) and (35) then dictates the enhancement of radiation emission at $\theta_B \simeq \arccos\{1/[\beta n(\omega)]\} = \theta_0$, i.e., at the Cherenkov angle θ_0, giving rise to a meaningful correlation between the emission angle and the radiation frequency ω within the Cherenkov-cone radiation pattern, in agreement with recent laser-plasma THz and microwave generation experiments [29–31]. Moreover, the condition of such an enhancement,

$$1 - \beta n(\omega)\cos\vartheta = 0, \quad (37)$$

recovers the universal Cherenkov phase-matching condition. Examples of such phase matching are found not only in Cherenkov radiation of THz field wave forms by laser filaments [12,17,32], but also in harmonic generation in waveguides and photonic crystals [38–42] and Cherenkov radiation by optical solitons [45–48]. Common to all these physically different phenomena is a signature conical radiation pattern of the nonlinear output–optical harmonics, soliton radiation, or THz emission. Notably, with regard to nonlinear-optical methods of THz generation, a reference to a Cherenkov emission cone dates all the way back to the pre-laser-filamentation era of pioneering research on THz generation in electro-optical materials [43,44]. Equations (28)–(35) reveal the connection between the conical radiation pattern of a nonlinear signal and Cherenkov-type phase matching between the radiation field and the source of radiation. Articulating this connection is Eq. (37). When rewritten as $v\cos\vartheta = c/n(\omega)$, this equation highlights that the radiation emission angle θ emerges as a result of constructive interference, i.e., a phase matching, between radiation wavelets emitted by the radiation source at each point of its trajectory.

VI. TRANSITION RADIATION SIGNATURES: ARGUMENTS FROM GINZBURG-FRANK TREATMENT

To gain deeper insight into the results of the previous sections, we examine a charge e that stays at rest at $z = 0$ for $t < 0$, but instantaneously starts to move in the positive direction along the z axis with a constant speed v at $t = 0$. The radiation field induced by such a charge at point r,

$$E_\theta = \frac{\sin\theta}{r} b(\beta, \theta)\delta\left(r - \frac{c}{n}t\right), \quad (38)$$

is oriented along the tangential to a sphere centered at $z = 0$ with a radius of ct/n [52,53]. In Fig. 1(b), this field is shown against the electrostatic field induced by the charge, illustrating Purcell's solution [52] for the field of a charge that instantaneously starts moving at $z = 0$.

Consider now a charge e that moves along the z axis with a constant speed v for $t < 0$, but instantaneously stops as it reaches $z = 0$ at $t = 0$. The field emitted by such a charge is equal in magnitude, but opposite in sign to the field E_ϑ as defined by Eq. (38).

It is instructive to examine Eq. (38) from a perspective of transition radiation—electromagnetic radiation emitted by a charged particle that traverses a boundary between two media, media A and B, with different dielectric properties [37]. As shown by Ginzburg and Frank [54,55], transition radiation can be understood as a sum $E_A + E_b$ of radiation, E_A, emitted by a charge that uniformly moves in medium A, but instantaneously stops at the boundary between A and B and radiation, E_B, emitted by a charge that instantaneously starts moving at the boundary between A and B and continues to move uniformly into medium B. The fields E_A and E_b cancel out only when A and B are identical in their dielectric properties. Since the structure of both radiation fields, E_A and E_b, is given by Eq. (38), we recognize E_ϑ defined by Eq. (38) as a signature of transition radiation.

Transition radiation aspects of the field E_ϑ as defined by Eq. (38) are, of course, inseparable from the signatures of bremsstrahlung, as the radiation of this field is due to charge acceleration, which in the considered setting happens to be infinite. Strong coupling between transition and radiation is revealed already by the original Ginzburg-Frank treatment of transition radiation, which operates with charges that instantaneously stop or start their motion [54,55]. The pertinence of transition radiation to radiation emitted by laser filaments has been earlier brought up by D'Amico *et al.* [32], who pointed out the significance of the finiteness of the filament length for the net radiation output and its properties.

Frequency ω enters into Eq. (38) only via the dispersion of $n(\omega)$ and $n_g(\omega)$. This is a consequence of an assumption of an infinite acceleration experienced by a charge that starts to

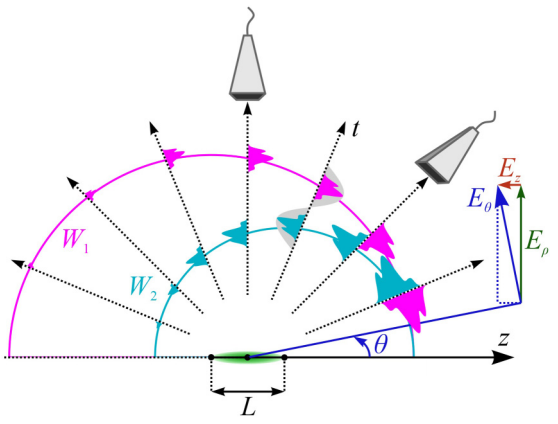

FIG. 3. Spatiotemporal field structure of radiation emitted by a laser filament of length L. Shown by pink and blue semicircles are the traveling waves of bremsstrahlung-transition radiation emitted by an electric charge as it instantaneously starts moving at $z = -L/2$ (W_1, pink) and instantaneously stops at $z = L/2$ (W_2, blue). Also shown is the field $\mathbf{E}_\theta = E_\theta \mathbf{e}_\theta$ expanded as a sum $\mathbf{E}_\theta = \mathbf{E}_z + \mathbf{E}_\rho$.

move, acquiring a constant speed v at $t = 0$. Any bandwidth limitation, e.g., due to a finite time interval within which the charge is allowed to start its motion or a cutoff frequency beyond which the gap between the dielectric functions of A and B closes, will add a frequency dependence to Eq. (38). To demonstrate this argument, we expand the Dirac delta function in Eq. (38) as

$$\delta\left(r - \frac{c}{n}t\right) = \frac{1}{c}\delta\left(t - \frac{nr}{c}\right) = \frac{1}{2\pi c}\int_{-\infty}^{\infty} \exp\left[i\omega\left(t - \frac{nr}{c}\right)\right]d\omega. \tag{39}$$

If the bandwidth is limited with a cutoff at ω_c, the $\delta(r–ct/n)$ in Eq. (38) is replaced by a frequency-dependent multiplier:

$$\frac{1}{2\pi c}\int_{-\omega_c}^{\omega_c} \exp\left[i\omega\left(t - \frac{nr}{c}\right)\right]d\omega = \frac{1}{\pi c}\frac{\sin\left[\omega_c\left(t - \frac{nr}{c}\right)\right]}{t - \frac{nr}{c}}. \tag{40}$$

When combined with Eqs. (38) and (39), Eq. (40) highlights that, even though Eq. (38) includes the radiation frequency ω only via the dispersion of the refractive index, $n = n(\omega)$, ω eventually finds a way to make it into Eq. (36) via bandwidth limitations inevitable in realistic laser-plasma settings.

VII. BREMSSTRAHLUNG-TRANSITION CHERENKOV RADIATION

The field defined by Eqs. (28)–(31) can now be understood as a superposition of two transition radiation fields emitted by a charge that instantaneously starts moving at $z = -L/2$ and continues to move with a constant speed v along the z axis until it instantaneously stops at $z = L/2$ [Fig. 2(a)]. As the charge starts moving at $z = -L/2$, it emits a transition radiation wave as described by the first term in Eq. (28), $W_1 = \Phi(z = -L/2)$, as shown in pink in Fig. 3. When the charge stops at $z = L/2$, it emits another, second wave of transition radiation, W_2, shown in blue in Fig. 3. Because the acceleration of the charge is now opposite in sign to the acceleration of a charge that starts its motion at $z = -L/2$, the polarity of W_2 is opposite to the polarity of W_1 (Fig. 3). This sign reversal is correctly reflected by the minus sign in front of the second term in Eq. (28), $W_2 = -\Phi(z = -L/2)$. Since the time it takes for the charge to travel the distance L is L/v, the waves W_1 and W_2 reach a detector oriented at an angle θ relative to the z axis with a time delay $\Delta t = L/v–(n/c)L\cos\vartheta = (L/v)(1–\beta n\cos\vartheta)$ (Fig. 3), giving rise to a phase shift $\varphi = \omega\Delta t = (\omega L/v)(1–\beta n\cos\vartheta)$ of the W_2 wave relative to W_1. It is precisely this phase shift that the $\exp(i\varphi)$ factor in Eq. (29) accounts for.

Remarkably, the radiation field E_ϑ, as defined by Eq. (38), bears the same polarization signatures as the Cherenkov radiation field in Eqs. (19)–(21) [Figs. 1(b) and 3]. Indeed, in spherical coordinates, the electric field radiated by a charge that instantaneously starts its motion or is instantaneously brought to a halt is completely described by a single polarization component E_ϑ. In cylindrical coordinates ρ, ϕ, z used in the Frank-Tamm treatment, this electric-field component is described in terms of two polarization components, E_ρ and E_z, defined by Eqs. (19) and (20), respectively, with $\mathbf{E}_\vartheta = E_\vartheta \mathbf{e}_\vartheta = \mathbf{E}_z + \mathbf{E}_\rho = E_z\mathbf{e}_z + E_\rho\mathbf{e}_\rho$, $\mathbf{e}_\vartheta$, $\mathbf{e}_z$, and $\mathbf{e}_\rho$ being the pertinent unit vectors.

As an important insight, Eqs. (33) and (34) offer two alternative, equally instructive pictures of secondary radiation by charge currents [Fig. 2(a)]. Indeed, the $[b(\beta, \vartheta)\sin\vartheta/R_0]^2$ angular profile in Eq. (33) is readily recognized as a signature of transition radiation [Eq. (36)], relating radiation by the electric current (22) to transition radiation by a charge that instantaneously starts moving near one of the ends of a filament and is instantaneously brought to a halt near the opposite filament end. The bremsstrahlung signature $J_B(\vartheta)$ in Eq. (34), on the other hand, reveals the bremsstrahlung connection of charge-current radiation as described by Eqs. (28)–(35). Making these two pictures equivalent is the laser-filament plasma-current radiation setting [Fig. 2(a)], in which transition radiation by a charge that instantaneously starts moving or instantaneously stops near one of the filament ends can be viewed as bremsstrahlung of a charge that picks up an abrupt, infinite acceleration that is parallel or antiparallel to its velocity [Fig. 2(a)].

VIII. INSIGHTS FROM DIPOLE RADIATION

As a trivial limit, with the filament length set equal to zero, $L = 0$, Eqs. (25)–(31) yield $A_\omega = 0$. Equation (28), however, offers an interesting perspective on this result, showing that the net radiation output vanishes for $L = 0$ as a result of $W_1 + W_2 = 0$ cancellation, which, in its turn, can be viewed as a cancellation of transition radiation wave W_1 (shown pink in Fig. 3) emitted by a charge that undergoes an instantaneous acceleration from $v = 0$ to $v \neq 0$ at some point $z = z_0$ along the filament by the opposite-polarity transition radiation wave W_2 (shown blue in Fig. 3), emitted by a charge that moves with a speed v, but is brought to a halt at the same point $z = z_0$.

Less straightforward is the limit of small, but nonzero L, such that $\omega L \ll v$, or, equivalently, $L \ll \beta\lambda/(2\pi)$, λ is the radiation wavelength. In this regime, $Q(\omega, \vartheta, L)$ becomes θ independent, $Q(\omega, \vartheta, L) \approx \omega L/(2v)$. The angular distribution

of radiation power density is then given by

$$S(\omega,\theta,L)\propto\frac{e^2\omega^2L^2}{4\pi^2c^3R_0^2}\sin^2\theta. \tag{41}$$

The spectral intensity of radiation as described by Eq. (41) is seen to be independent of v/c, recovering a signature, $(k_0d)^2\sin^2\vartheta$ p-wave radiation pattern [pink line in Fig. 2(a)], typical of radiation by an electric dipole with a dipole moment $\mathbf{d}=eL\mathbf{e}_z$, where $\mathbf{e}_z$ is the unit vector along the z axis [Fig. 2(a)]. The buildup of radiation from longer-L filaments can now be viewed as an interference of radiation fields emitted by elementary electric dipoles arranged along the filament [Fig. 2(a)] with the spectral intensity of radiation by each such dipole as described by Eq. (41). Indeed, Eq. (3) with the source term $\mathbf{j}_\omega$ as defined by Eq. (23) is equivalent to

$$\nabla^2\mathbf{A}_\omega+k_0^2n^2\mathbf{A}_\omega=-\frac{4\pi i\omega}{c}\mathbf{P}_\omega, \tag{42}$$

with a fictitious polarization

$$\mathbf{P}_\omega=-\frac{ie}{2\pi\omega}\frac{\mathbf{v}}{v}\exp\left(i\frac{\omega}{v}z\right)\delta(x)\delta(y). \tag{43}$$

The solution to Eq. (42) with the source term in the form of Eq. (43) recovers Eq. (25). Each Fourier component of radiation emitted by the current (22) can thus be found as the field emitted by a linear array of electric-dipole harmonic oscillators arranged along the line of the current [Fig. 2(a)]. Since radiation emitted by each dipole is independent of v/c, the total radiation field emitted by a finite-L filament is nonvanishing regardless of whether the charges forming the current are superluminal, $v>c/n$, or subluminal, $v<c/n$. Moreover, the crossover from $v>c/n$ to $v<c/n$ in Eqs. (24)–(35) is continuous for any finite L.

The Cherenkov effect with its signature sharp emission cone [Fig. 1(a)] is recovered via $\lim_{L\to\infty}[Q(\omega,\theta,L)]=\pi\delta(1-\beta n\cos\vartheta)$ in Eq. (27), leading to $A_\omega\propto\delta(1-\beta n\cos\vartheta)$. The radiation output in this regime vanishes unless $v>c/n$ and $\cos\vartheta=\cos\vartheta_0=1/(\beta n)$, accurately reproducing all the properties of Cherenkov radiation by superluminal, $v>c/n$ charges. As the edges of the filament with their transition or bremsstrahlung radiation are now at an infinite L, the Cherenkov radiation effect remains the only source of radiation.

While a superluminal, $v>c/n$ charge (1) moving along an infinite trajectory [Eq. (2)] can radiate only at a well-defined angle $\cos\vartheta_0=1/(\beta n)$ [see Eqs. (12)–(18)], a charge on a finite-length trajectory radiates within a range of angles [Fig. 2(a)], giving rise to a radiation pattern [the black line in Fig. 2(a)] whose angular width $\Delta\vartheta$ can be found from $\omega L[1-\beta n\cos(\vartheta_0+\Delta\vartheta)]=2v\pi$, leading to $nL[\cos\vartheta_0-\cos(\vartheta_0+\Delta\vartheta)]=\lambda$. For long filaments with $L/\lambda\gg1$, this equation yields $\Delta\vartheta\approx\lambda/(nL\sin\vartheta_0)$. As the speed v becomes less than c/n, the main maximum of $Q(\omega,\vartheta,L)$, $Q(\omega,\vartheta,L)=(\pi/\beta)(L/\lambda)$ with $\cos\vartheta=\cos\vartheta_0=1/(\beta n)$, is no longer achieved for real θ, yet the radiation output, as can be seen from Eqs. (25)–(32), remains nonzero as long as L is finite.

IX. EMISSION CONE, LOW-FREQUENCY CUTOFF, AND PHASE-MATCHED NONLINEAR POLARIZATION

The Cherenkov emission cone can thus be viewed as an emergent property of radiation by an array of electric dipoles $\mathbf{d}$ [Fig. 2(a)]. As the length of this array, L, increases from $L\ll\beta\lambda/(2\pi)$ to $L\gg\beta\lambda/(2\pi)$, the far-field radiation pattern is gradually transformed from a figure of eight angular distributions, typical of radiation by a single dipole [pink line in Fig. 2(a)], to a well-resolved $\delta(1-\beta n\cos\theta)$ Cherenkov emission cone. Radiation in the forward direction, i.e., along the z axis, is suppressed for any L by $\sin^2\vartheta$ in Eqs. (32)–(35) [Fig. 2(a)]. In the limit of $2\pi L\gg\beta\lambda$, the far-field radiation pattern is independent of L. The properties of radiation emitted by a laser filament in this regime are controlled by the v/c ratio and the frequency dependence of the refractive index, $n=n(\omega)$. For filaments of intermediate lengths, however, L emerges as a key parameter that defines, via Eqs. (25)–(27), the spatial scale within which the radiation fields emitted by individual dipoles can add up coherently, thus setting a significant wavelength scale for radiation emission by moving charges, plasma currents, and laser filaments, with a long-wavelength cutoff set, in accordance with Eq. (27), at around $\lambda_f\simeq Ln|\cos\vartheta_0-\cos\vartheta|$. With $\beta n\simeq1$ and $n\simeq1$, λ_f becomes $\lambda_f\simeq L|1-\cos\vartheta|$, recovering the $\lambda/2$-antenna result $\lambda_f\simeq2L$ for $\vartheta\simeq\pi$.

The emergence of the new frequency scale $\omega_f=2\pi c/\lambda_f\sim c/L$ offers interesting insights into the results of laser-filamentation experiments, which show that the broadband supercontinua emitted by laser filaments often extend to the sub-THz-to-microwave range, thus stretching well beyond the standard $\omega_m\sim1/\tau_0$ cutoff, as dictated by the pulse width of the laser driver τ_0. In a physical setting of the bremsstrahlung-transition Cherenkov radiation as described by Eqs. (23)–(33), these results are naturally explained in terms of coherent combining of radiation waves emitted by elementary dipoles along the filament length [Fig. 2(a)]. For each radiation wavelength λ, these waves, as Eq. (27) shows, can add up in phase only within the length $L\simeq\lambda/2$, giving rise to the $\lambda_f\simeq2L$ cutoff. The low-frequency radiation output thus builds up as L^2 for short filaments, with $L\ll\beta\lambda/(2\pi)$, but tends to saturate as L approaches $\beta\lambda/(2\pi)$. This scaling of $S(\omega,\theta,L)$ with L bears a close resemblance with a textbook picture of phase-matching-sensitive wave mixing described in terms of bound-state nonlinear polarization [56]. Moreover, Eqs. (25)–(33) are consistent with conical emission patterns of THz, sub-THz, and microwave radiation observed in laser-filamentation experiments, where the radiation output, detected within a limited bandwidth as dictated by a finite passband of the detection system, is a nonmonotonic function of the detection angle, changing with the gas pressure, beam-focusing geometry, and other factors influencing the filament length [27–31]. The physical model of Eqs. (23)–(33) thus offers a unified framework within which the nonlinear-optical response of moving charges and plasma currents, such as those found in laser filaments, can be treated on equal footing with phase-matching-sensitive light-matter interactions induced via bound-state nonlinear polarization.

X. CONCLUSION

To summarize, we have shown that the edge effects, inherent in the LF setting, tend to couple Cherenkov radiation emitted by charge currents to bremsstrahlung and transition radiation, making these three types of radiation physically indistinguishable. Resorting to an evanescent-field extension of the Cherenkov effect to subluminal electric currents, we have provided a unified description of low-frequency radiation by sub- and superluminal plasma currents with a continuous analytical crossover from the superluminal to the subluminal picture of bremsstrahlung-transition Cherenkov radiation. In this laser-plasma interaction scenario, long-wavelength radiation builds up outside the laser plasma, unfolding at spatial scales much larger than the transverse size of the LP source. Central to this physical setting is an interference of electromagnetic traveling waves emitted by impulsively driven transient currents near the LP or LF edges, which combine into a far-field radiation pattern whose low-frequency cutoff is defined by the LP or LF length and whose spectral and spatial properties are in agreement with experimental studies. In a more general context, the analysis presented in this study suggests a unified framework within which the nonlinear-optical response of moving charges and plasma currents, such as those found in laser filaments, can be treated on equal footing with phase-matching-sensitive light-matter interactions induced via bound-state nonlinear polarization.

ACKNOWLEDGMENTS

This research was supported in part by the Russian Foundation for Basic Research (Projects No. 18-29-20031 and No. 19-02-00473), Russian Science Foundation (Project No. 20-12-00088—ultrabroadband optical science), Ministry of Science and Higher Education of the Russian Federation (Project No. 075-15-2020-801), and the Welch Foundation (Grant No. A-1801-20180324).

[1] A. Couairon and A. Mysyrowicz, Phys. Rep. **441**, 47 (2007).
[2] L. Bergé, S. Skupin, R. Nuter, J. Kasparian, and J.-P. Wolf, Rep. Prog. Phys. **70**, 1633 (2007).
[3] M. Durand, A. Jarnac, A. Houard, Y. Liu, S. Grabielle, N. Forget, A. Durécu, A. Couairon, and A. Mysyrowicz, Phys. Rev. Lett. **110**, 115003 (2013).
[4] A. V. Mitrofanov, A. A. Voronin, M. V. Rozhko, D. A. Sidorov-Biryukov, A. B. Fedotov, A. Pugžlys, V. Shumakova, S. Ališauskas, A. Baltuška, and A. M. Zheltikov, Optica **4**, 1405 (2017).
[5] A. M. Zheltikov, J. Opt. Soc. Am. B **36**, A168 (2019).
[6] J. Kasparian, M. Rodriguez, G. Méjean, J. Yu, E. Salmon, H. Wille, R. Bourayou, S. Frey, Y.-B. André, A. Mysyrowicz, R. Sauerbrey, J.-P. Wolf, and L. Wöste, Science **301**, 61 (2003).
[7] F. Silva, D. R. Austin, A. Thai, M. Baudisch, M. Hemmer, D. Faccio, A. Couairon, and J. Biegert, Nat. Commun. **3**, 807 (2012).
[8] H. Liang, P. Krogen, R. Grynko, O. Novak, C.-L. Chang, G. J. Stein, D. Weerawarne, B. Shim, F. X. Kärtner, and K.-H. Hon, Opt. Lett. **40**, 1069 (2015).
[9] A. M. Zheltikov, Phys. Usp. **49**, 605 (2006).
[10] A. Couairon, M. Franco, A. Mysyrowicz, J. Biegert, and U. Keller, Opt. Lett. **30**, 2657 (2005).
[11] A. V. Mitrofanov, A. A. Voronin, D. A. Sidorov-Biryukov, S. I. Mitryukovsky, A. B. Fedotov, E. E. Serebryannikov, D. V. Meshchankin, V. Shumakova, S. Ališauskas, A. Pugžlys, V. Ya, Panchenko, A. Baltuška, and A. M. Zheltikov, Optica **3**, 299 (2016).
[12] P. Sprangle, J. Peñano, B. Hafizi, and C. Kapetanakos, Phys. Rev. E **69**, 066415 (2004).
[13] C. D'Amico, A. Houard, M. Franco, B. Prade, A. Mysyrowicz, A. Couairon, and V. T. Tikhonchuk, Phys. Rev. Lett. **98**, 235002 (2007).
[14] K. Y. Kim, A. J. Taylor, J. H. Glownia, and G. Rodriguez, Nat. Photonics **2**, 605 (2008).
[15] N. Karpowicz and X.-C. Zhang, Phys. Rev. Lett. **102**, 093001 (2009).
[16] A. M. Zheltikov, J. Phys. B: At. Mol. Opt. Phys. **50**, 092001 (2017).
[17] I. Thiele, R. Nuter, B. Bousquet, V. Tikhonchuk, S. Skupin, X. Davoine, L. Gremillet, and L. Bergé, Phys. Rev. E **94**, 063202 (2016).
[18] N. Horiuchi, Nat. Photonics **4**, 140 (2010).
[19] M. Schultze, E. M. Bothschafter, A. Sommer, S. Holzner, W. Schweinberger, M. Fieß, M. Hofstetter, R. Kienberger, V. Apalkov, V. S. Yakovlev, M. I. Stockman, and F. Krausz, Nature (London) **493**, 75 (2012).
[20] M. Garg, M. Zhan, T. T. Luu, H. Lakhotia, T. Klostermann, A. Guggenmos, and E. Goulielmakis, Nature (London) **538**, 359 (2016).
[21] G. Vampa, T. J . Hammond, M. Taucer, X. Ding, X. Ropagnol, T. Ozaki, S. Delprat, M. Chaker, N. Thiré, B. Schmidt, F. Légaré, D. Klug, A. Naumov, D. Villeneuve, A. Staudte, and P. Corkum, Nat. Photonics **12**, 465 (2018).
[22] E. A. Nanni, W. R. Huang, K.-H. Hong, K. Ravi, A. Fallahi, G. Moriena, R. J. Dwayne Miller, and F. X. Kärtner, Nat. Commun. **6**, 8486 (2015).
[23] T. Kampfrath, A. Sell, G. Klatt, A. Pashkin, S. Mährlein, T. Dekorsy, M. Wolf, M. Fiebig, A. Leitenstorfer, and R. Huber, Nat. Photonics **5**, 31 (2011).
[24] F. Langer, C. P. Schmid, S. Schlauderer, M. Gmitra, J. Fabian, P. Nagler, C. Schüller, T. Korn, P. G. Hawkins, J. T. Steiner, U. Huttner, S. W. Koch, M. Kira, and R. Huber, Nature (London) **557**, 76 (2018).
[25] A. A. Lanin, E. A. Stepanov, A. B. Fedotov, and M A., Zh. Opt. **4**, 516 (2017).
[26] S. Tzortzakis, G. Méchain, G. Patalano, Y.-B. André, B. Prade, M. Franco, A. Mysyrowicz, J.-M. Munier, M. Gheudin, G. Beaudin, and P. Encrenaz, Opt. Lett. **27**, 1944 (2002).
[27] Y. Brelet, A. Houard, G. Point, B. Prade, L. Arantchouk, J. Carbonnel, Y.-B. Andre, M. Pellet, and A. Mysyrowicz, Appl. Phys. Lett. **101**, 264106 (2012).
[28] B. Forestier, A. Houard, M. Durand, Y.-B. André, B. Prade, J.-Y. Dauvignac, F. Perret, C. Pichot, M. Pellet, and A. Mysyrowicz, Appl. Phys. Lett. **96**, 141111 (2010).

[29] A. Englesbe, J. Elle, R. Reid, A. Lucero, H. Pohle, M. Domonkos, S. Kalmykov, K. Krushelnick, and A. Schmitt-Sody, Opt. Lett. **43**, 4953 (2018).
[30] A. V. Mitrofanov, D. A. Sidorov-Biryukov, M. M. Nazarov, A. A. Voronin, M. V. Rozhko, A. D. Shutov, S. V. Ryabchuk, E. E. Serebryannikov, A. B. Fedotov, and A. M. Zheltikov, Optica **7**, 15 (2020).
[31] A. V. Mitrofanov, D. A. Sidorov-Biryukov, M. M. Nazarov, A. A. Voronin, M. V. Rozhko, A. B. Fedotov, and A. M. Zheltikov, Opt. Lett. **46**, 1081 (2021).
[32] C. D'Amico, A. Houard, S. Akturk, Y. Liu, J. Le Bloas, M. Franco, B. Prade, A. Couairon, V. Tikhonchuk, and A. Mysyrowicz, New J. Phys. **10**, 013015 (2007).
[33] I. Frank and I. Tamm, C. R. (Dokl.) Acad. Sci. URSS **14**, 109 (1937).
[34] I. Tamm, J. Phys. USSR **1**, 439 (1939).
[35] L. D. Landau, E. M. Lifshitz, and L. P. Pitaevskii, *Electrodynamics of Continuous Media*, 2nd ed. (Butterworth-Heinemann, Oxford, 1984).
[36] P. A. Cherenkov, Phys. Rev. **52**, 378 (1937).
[37] J. D. Jackson, *Classical Electrodynamics*, 3rd ed. (Wiley, New York, 1999).
[38] P. Tien, R. Ulrich, and R. Martin, Appl. Phys. Lett. **17**, 447 (1970).
[39] Y. Zhang, Z. D. Gao, Z. Qi, S. N. Zhu, and N. B. Ming, Phys. Rev. Lett. **100**, 163904 (2008).
[40] A. M. Zheltikov, Phys. Rev. A **72**, 043812 (2005).
[41] A. A. Ivanov, D. Lorenc, I. Bugar, F. Uherek, E. E. Serebryannikov, S. O. Konorov, M. V. Alfimov, D. Chorvat, and A. M. Zheltikov, Phys. Rev. E **73**, 016610 (2006).
[42] Y. Sheng, S. M . Saltiel, W. Krolikowski, A. Arie, K. Koynov, and Y. S . Kivshar, Opt. Lett. **35**, 1317 (2010).
[43] D. H. Auston, Appl. Phys. Lett. **43**, 713 (1983).
[44] D. H. Auston, K. P. Cheung, J. A. Valdmanis, and D. A. Kleinman, Phys. Rev. Lett. **53**, 1555 (1984).
[45] N. Akhmediev, and M. Karlsson, Phys. Rev. A **51**, 2602 (1995).
[46] J. M. Dudley, G. Genty, and S. Coen, Rev. Mod. Phys. **78**, 1135 (2006).
[47] A. M. Zheltikov, Phys. Usp. **50**, 705 (2007).
[48] G. Agrawal, *Nonlinear Fiber Optics*, 6th ed. (Academic, New York, 2019).
[49] J. D. Lawson, Am. J. Phys. **33**, 1002 (1965).
[50] D. J. Griffiths, *Introduction to Electrodynamics*, 3rd ed. (Prentice-Hall, Upper Saddle River, NJ, 1999).
[51] A. V. Mitrofanov, A. A. Voronin, M. V. Rozhko, D. A. Sidorov-Biryukov, M. M. Nazarov, A. B. Fedotov, and A. M. Zheltikov, ACS Photonics **8**, 1988 (2021).
[52] E. M. Purcell, Electricity and Magnetism, *Berkeley Physics Course* (McGraw-Hill, New York, 1965), Vol. 2.
[53] B. M. Bolotovskii and A. V. Serov, Phys. Usp. **52**, 487 (2009).
[54] V. L. Ginzburg and I. M. Frank, Zh. Eksp. Teor. Fiz. **16**, 15 (1946).
[55] V. L. Ginzburg, Phys. Usp. **39**, 973 (1996).
[56] Y. R. Shen, *The Principles of Nonlinear Optics* (Wiley-Interscience, New York, 1984).